Nigerian Journal of Physics (NJP)
ISSN online: 3027-0936
ISSN print: 1595-0611
DOI: https://doi.org/10.62292/njp.v35(s).2026.727
Volume 35(S), 2026

Computational Modelling of B_0 Field Strength Effects on Stroke MRI Image Quality: 0.5T vs 1.5T

[1,2]Dauda Biodun Amuda, *[1]Oluwasegun Daniel Oyinloye, [2,3]Temitope Olugbenga Bello, [2]Victor Olufemi Oyedepo, [4]Godwin Inalegwu Ogbole, [4]Adesola Emmanuel Adepoju, [5]Ismail Oyeleke Olarinoye, [6]Samson Damilola, [7]Olanike Funke Amuda, [8]Oluwole Ogundoyin and [9]Omowonuola Ogundoyin

[1]Department of Pure and Applied Physics, LAUTECH, Ogbomoso, Nigeria.
[2]Department of Radiology, LAUTECH Teaching Hospital, Ogbomoso, Nigeria.
[3]Department of Radiology, University of the Gambia, Gambia.
[4]Department of Radiology, University of Ibadan, Ibadan, Nigeria.
[5]Department of Physics, Federal University of Technology, Minna, Nigeria.
[6]Department of Physics, University of Abuja, Abuja, Nigeria.
[7]Department of Sociology (Health Care Option), LAUTECH, Ogbomoso, Nigeria.
[8]Stemax Consult Healthcare Services, Milton Keynes, England.
[9]Bioluminux Clinical Research, Milton Keynes, England.

*Corresponding Author's Email: odoyinloye@pgschool.lautech.edu.ng

Keywords:
Magnetic Resonance Imaging, Ischemic Stroke, Magnetic Field Strength, Computational Simulation, Image Quality

Submitted: 21 Aug. 2026
Accepted: 07 Sept. 2026
Published: 02 July 2026

ABSTRACT

Ischemic stroke outcomes depend on rapid, accurate neuroimaging, and magnetic resonance imaging (MRI) performance is governed by static magnetic field strength. Low-field 0.5 Tesla systems form a substantial share of installed MRI infrastructure in Nigeria and similar resource-limited settings, yet their comparative performance for stroke imaging has not previously been examined using a physics-based computational framework. This study modeled the effects of field strength on MRI image quality in ischemic stroke imaging, comparing 0.5 Tesla and 1.5 Tesla. A digital brain phantom (256 by 256 pixels) was constructed with six tissue compartments, including cerebrospinal fluid and a simulated ischemic stroke lesion in the left middle cerebral artery territory. Magnetic field distributions were computed using a susceptibility-perturbation finite element approximation in Python, followed by spin-echo signal generation, k-space synthesis, and image reconstruction, evaluated using signal-to-noise ratio, contrast-to-noise ratio, normalized mutual information, and image sharpness across thirty noise realizations per field strength. At 1.5 Tesla, signal-to-noise ratio increased by 72.41% and contrast-to-noise ratio by 73.07% relative to 0.5 Tesla, while image sharpness decreased by 32.38% relative to 0.5 Tesla; both metrics changed monotonically and consistently between the two field strengths examined. The simulated stroke lesion satisfied the Rose detectability criterion at both field strengths, with a substantially larger safety margin at 1.5 Tesla (+169.8%) than at 0.5 Tesla (+55.9%). These findings indicate that 1.5 Tesla is the superior field strength for stroke MRI across most evaluated criteria, and the two-point interpolation relationships derived between 0.5T and 1.5T provide a preliminary computational reference for protocol comparison between these two field strengths in resource-limited radiology practice.

INTRODUCTION

Ischemic stroke is a major neurological disorder resulting from acute cerebral blood flow reduction or cessation. Rapid and accurate neuroimaging is a determinant of clinical outcome, as the extent of irreversible infarction grows with time from onset (Salaudeen et al., 2024; Al-Salahat, 2025).

Magnetic resonance imaging (MRI) provides high soft-tissue contrast without ionizing radiation and detects ischemic changes earlier than computed tomography,

particularly through diffusion-weighted imaging sequences sensitive to cytotoxic edema (Gagliardo et al., 2025; Yuen et al., 2022). Rapid, reliable stroke imaging is therefore of direct social and clinical value, underpinning time-critical treatment decisions in acute stroke care.

The static magnetic field strength (B_0) governs MRI signal intensity, tissue contrast, and spatial resolution. Higher B_0 increases equilibrium magnetization and, in principle, the available signal for image formation. However, increasing B_0 also amplifies magnetic susceptibility differences between brain tissues, air-tissue interfaces, and blood products, generating spatially varying field perturbations that manifest as geometric distortion, signal dropout, and reduced image sharpness (Bhat et al., 2021; Mahendran et al., 2022).

In Nigeria and similar resource-limited settings, low-field MRI systems operating at 0.5T constitute a significant proportion of installed clinical infrastructure. Most existing comparative studies treat field strength as a fixed system attribute and lack a physics-based computational framework that explicitly models B_0 distributions within brain geometry and links these distributions to measurable image-quality metrics relevant to stroke diagnosis (Kravchenko et al., 2025; Stockmann & Wald, 2018). This represents the scientific gap this study addresses.

While the near-linear scaling of SNR with B_0 is well established in MRI physics, the contribution of this study lies in translating that established relationship into a stroke-lesion-specific detectability framework: quantifying the Rose-criterion safety margin for an ischemic lesion at each field strength and deriving two-point interpolation relationships that link B_0 to clinically actionable image-quality thresholds at the two field strengths examined.

A five-stage computational simulation pipeline was developed to model B_0 field distributions, generate synthetic spin-echo MRI images, and evaluate four quantitative image-quality metrics at 0.5T and 1.5T. The aims were to: (1) simulate magnetic field distributions in human brain geometry; (2) quantify the effect of field strength variation on SNR and CNR; (3) evaluate ischemic lesion detectability using the Rose criterion; and (4) derive two-point interpolation relationships between B_0 and image-quality metrics for the two field strengths examined.

MATERIALS AND METHODS

Study Design

This was a quantitative, physics-based computational simulation study comparing MRI image quality at two static magnetic field strengths (0.5T and 1.5T) using a controlled, repeated-realization simulation design conducted entirely in silico using Python (NumPy, SciPy).

Digital Brain Phantom

A digital brain phantom (256 × 256 pixels) was constructed with six tissue compartments: background (air), skull, white matter (WM), gray matter (GM), cerebrospinal fluid (CSF), and an ischemic stroke lesion in the left middle cerebral artery territory. Each compartment was assigned magnetic susceptibility (χ), proton density (ρ), T_1, and T_2 values drawn from published relaxometry literature (Gracien et al., 2016; Siemonsen et al., 2017). The stroke lesion was assigned elevated T_1 and T_2 values relative to surrounding WM, representing the increased tissue water content of cytotoxic edema. Tissue property values are presented in Table 1. CSF occupies the ventricular space nested within the white matter compartment, with the lesion positioned separately in the left middle cerebral artery territory.

Magnetic Field Simulation

Magnetic field distributions at each field strength were computed using a susceptibility-perturbation finite element approximation implemented in Python. Local flux density at each voxel was modeled as $B_{local}(r) = B_0 + B_0 \cdot \chi(r)/3$, where $\chi(r)$ is the local magnetic susceptibility. Gaussian spatial smoothing was applied to approximate dipolar field spreading, with field simulations run independently at each field strength.

MRI Signal Simulation and Image Quality Metrics

MRI signal intensity was simulated using the spin-echo signal equation with repetition time TR = 2000 ms and echo time TE = 80 ms, corresponding to a T_2-weighted spin-echo sequence used in clinical stroke imaging. Synthetic k-space data were generated by two-dimensional discrete Fourier transformation of the signal map, with noise added at a level scaled inversely with B_0, and images recovered by inverse Fourier transformation. Thirty independent noise realizations were generated at each field strength. Four image-quality metrics were computed from each reconstructed image: signal-to-noise ratio (SNR), contrast-to-noise ratio (CNR) between the lesion and surrounding WM, normalized mutual information (NMI) relative to a noiseless reference image, and image sharpness computed as the sum of Sobel gradient magnitudes. Lesion detectability was assessed using the Rose criterion, which specifies that reliable human observer detection requires CNR $\geq$ 5 (Barrett & Myers, 2004).

Statistical Analysis

Descriptive statistics (mean, standard deviation) were computed for each metric across the 30 noise realizations. One-way analysis of variance (ANOVA) tested for statistically significant differences between field-strength groups at $\alpha = 0.05$. Because image-quality metrics were assessed at only two discrete field strengths, a two-point linear interpolation connecting the mean value at 0.5T

and 1.5T was constructed for each metric. A line fitted to two points is exact by definition, so R^2 was not used to validate linearity; the resulting equations were treated strictly as interpolants between the two calibration points rather than as regression models generalizable across the field-strength continuum. All statistical analyses were implemented in Python using NumPy and SciPy libraries.

Ethical Considerations

This study involved computational simulation only, using a synthetic digital brain phantom with no real patient data. No human participants or animal subjects were involved at any stage, and no institutional ethics committee approval or waiver was required.

RESULTS AND DISCUSSION

Brain Phantom and Tissue Parameters

The digital brain phantom reproduced the spatial arrangement of six brain tissue compartments, including a distinct cerebrospinal fluid (CSF) compartment nested within the white matter, and a stroke lesion positioned in the left middle cerebral artery territory. CSF had the longest T_2 (2.200 s) and the stroke lesion had elevated T_1 (1.100 s) and T_2 (0.130 s) relative to WM, consistent with edematous tissue properties. Tissue parameters are listed in Table 1.

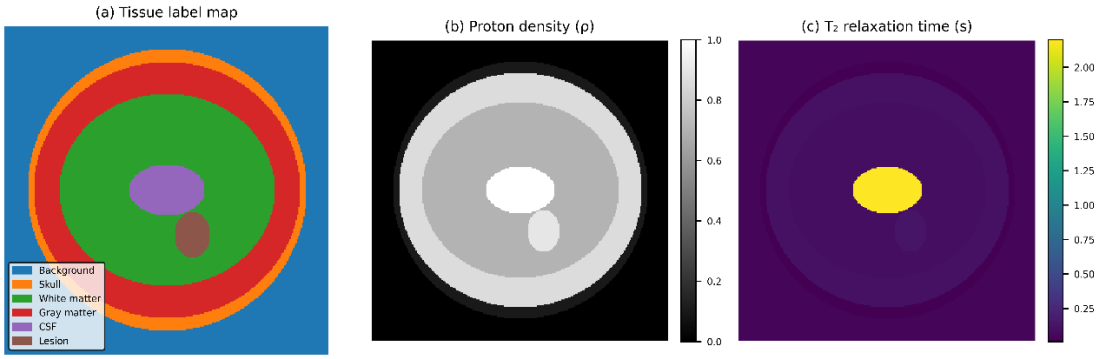

Figure 1: Digital Brain Phantom: (a) Tissue Label Map Showing Six Tissue Compartments Including the CSF-Filled Ventricular Space, (b) Proton Density Map (ρ), (c) T_2 Relaxation Time Map

Magnetic Field Distributions

Absolute field inhomogeneity increased from 0.0362 µT at 0.5T to 0.0993 µT at 1.5T, a 174.0% rise. Fractional inhomogeneity was comparable at both field strengths (0.0725 ppm vs 0.0662 ppm). The largest field deviations occurred at the skull-brain interface and CSF-WM boundaries. Field statistics are summarized in Table 2.

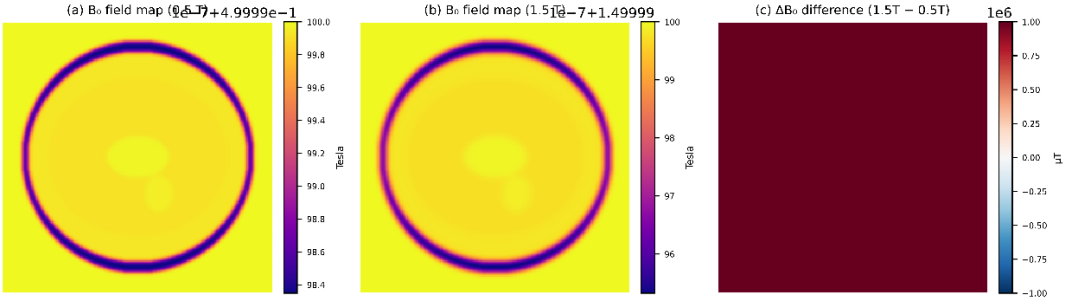

Figure 2: Simulated B_0 Magnetic Field Distributions: (a) 0.5T, (b) 1.5T, (c) Absolute Field Difference Map (1.5T − 0.5T)

Reconstructed MRI Images and Image Quality Metrics

Visual inspection of reconstructed images showed improved tissue boundary definition and lesion-background contrast at 1.5T. Table 3 presents descriptive statistics for all four metrics. At 1.5T, SNR increased by 72.41% (13.243±0.078 vs 22.832±0.150; $F=96,516.82$; $p<0.001$) and CNR increased by 73.07% (7.796±0.074 vs 13.491±0.117; $F=50,569.49$; $p<0.001$). NMI increased by 5.86% (1.2447±0.0014 vs 1.3176±0.0017; $F=31,424.65$; $p<0.001$). Image sharpness decreased by 32.38% ($9,079.4\times10^3$ vs $6,139.5\times10^3$ gradient units; $F=214,887.47$; $p<0.001$).

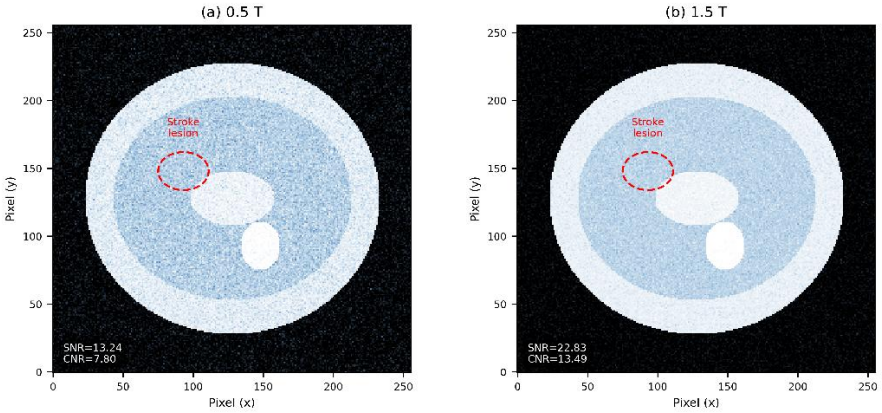

Figure 3: Reconstructed Spin-Echo MRI Images at (a) 0.5T and (b) 1.5T. Red Dashed Ellipse Delineates the Simulated Ischemic Stroke Lesion in the Left Middle Cerebral Artery Territory

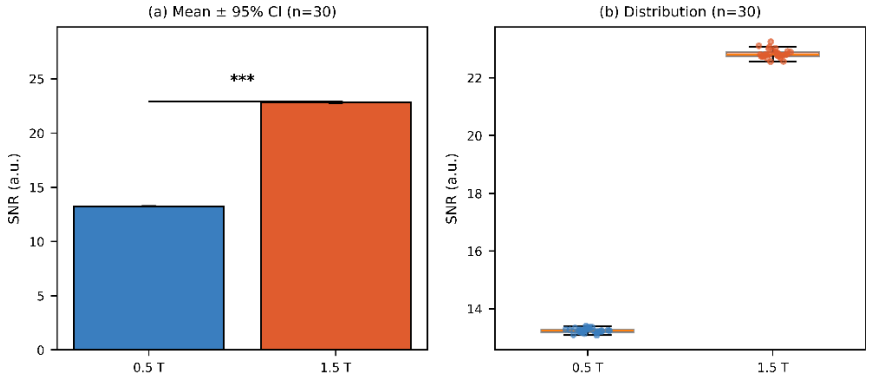

Figure 4a: Signal-to-Noise Ratio (SNR) at 0.5T and 1.5T: (a) Mean ± 95% CI Bar Chart (n=30); (b) Distribution with Individual Data Points. ***p<0.001

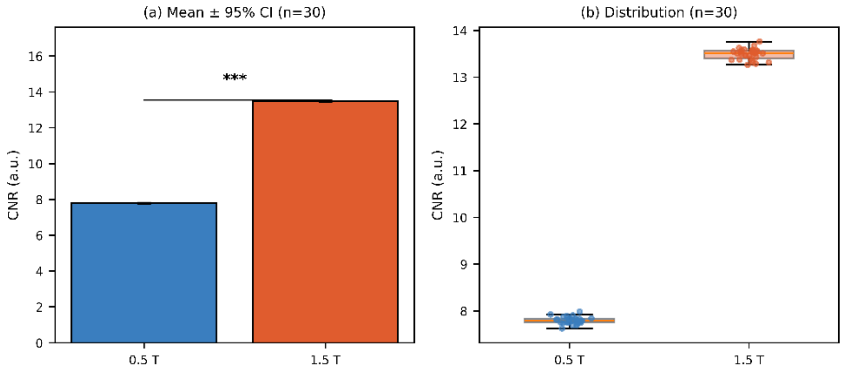

Figure 4b: Contrast-to-Noise Ratio (CNR) at 0.5T and 1.5T: (a) Mean ± 95% CI Bar Chart (n=30); (b) Distribution with Individual Data Points. ***p<0.001

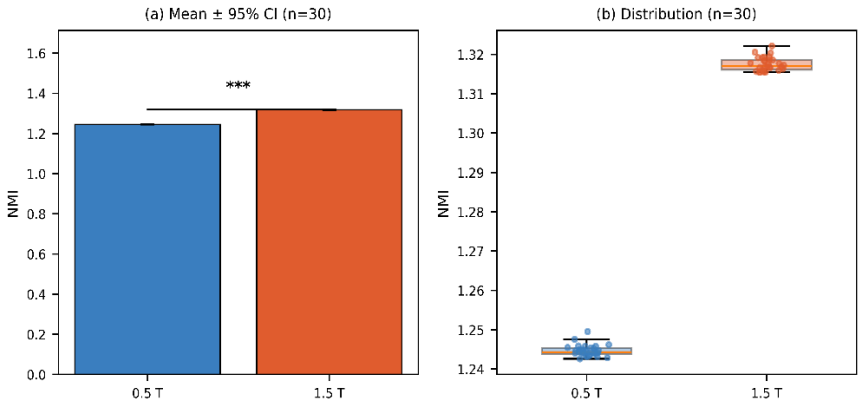

Figure 4c: Normalized Mutual Information (NMI) at 0.5T and 1.5T: (a) Mean ± 95% CI Bar Chart (n=30); (b) Distribution with Individual Data Points. ***p<0.001

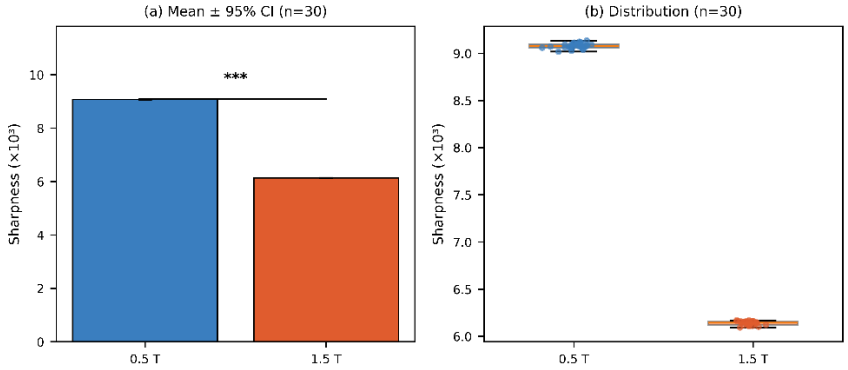

Figure 4d: Image Sharpness (×10³) at 0.5T and 1.5T: (a) Mean ± 95% CI Bar Chart (n=30); (b) Distribution with Individual Data Points. ***p<0.001

Lesion Detectability and Two-Point Interpolation

The Rose criterion (CNR ≥ 5) was met at both field strengths. The margin above the threshold was +55.9% at 0.5T (CNR=7.796) and +169.8% at 1.5T (CNR=13.491), a margin ratio of 3.04. Two-point linear interpolation between the 0.5T and 1.5T means was performed for each metric, with the resulting equations presented in Table 4. For a target CNR of 10, the recommended working threshold for reliable small-infarct detection, linear interpolation between the two field strengths yields an estimated B_0 of approximately 0.887T; this figure assumes linear behavior between the two calibration points and has not been validated against intermediate field strengths.

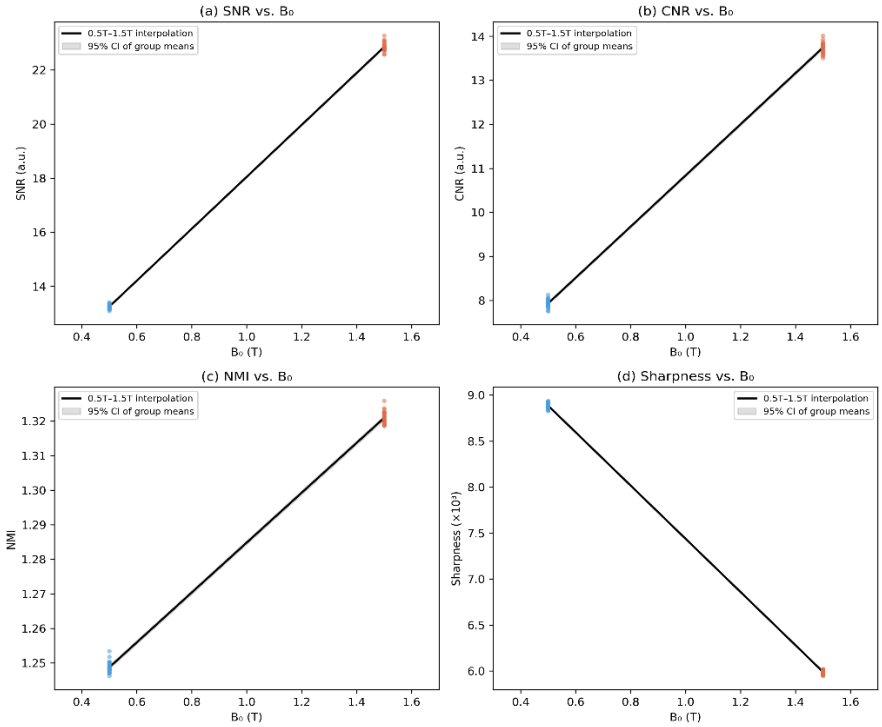

Figure 5: Two-Point Linear Interpolation of Image Quality Metrics Against B_0 Field Strength: (a) SNR, (b) CNR, (c) NMI, (d) Sharpness. Solid Line: Interpolation Between the 0.5T and 1.5T Means; Shaded Band: 95% Confidence Interval of the Group Means

Table 1: Electromagnetic and MRI Tissue Properties Used in the Digital Brain Phantom

Tissue region	χ (ppm)	Proton density (ρ)	T_1 (s)	T_2 (s)
Background (air)	0.000	0.00	1.000	0.050
Skull	−1.000	0.10	0.500	0.010
White matter	−0.053	0.70	0.780	0.087
Gray matter	−0.040	0.86	1.350	0.110
CSF	−0.010	1.00	4.500	2.200
Stroke lesion	−0.025	0.90	1.100	0.130

CSF, Cerebrospinal fluid; χ, Magnetic Susceptibility; ρ, Proton Density Normalized to Free Water

Table 2: Simulated B_0 Field Inhomogeneity Statistics within the Brain Phantom

Field strength (T)	Std. dev. (μT)	Min B_local (T)	Max B_local (T)	Inhomogeneity (ppm)
0.5	0.0362	0.4999998	0.5000000	0.0725
1.5	0.0993	1.4999995	1.5000000	0.0662

Table 3: Image Quality Metrics at 0.5T and 1.5T (n=30 per Group, Mean ± SD)

Metric	0.5T mean (±SD)	1.5T mean (±SD)	% change	F-statistic	p-value
SNR	13.243 (±0.078)	22.832 (±0.150)	+72.41%	96,516.82	<0.001
CNR	7.796 (±0.074)	13.491 (±0.117)	+73.07%	50,569.49	<0.001
NMI	1.2447 (±0.0014)	1.3176 (±0.0017)	+5.86%	31,424.65	<0.001
Sharpness (×10³)	9,079.4 (±27.9)	6,139.5 (±20.7)	−32.38%	214,887.47	<0.001

SNR, Signal-to-Noise Ratio; CNR, Contrast-to-Noise Ratio; NMI, Normalized Mutual Information; SD, Standard Deviation

Table 4: Two-Point Linear Interpolation Equations: Image Quality Metrics as a Function of B_0 (0.5T and 1.5T Only; not Validated as Predictive Regression Models Across Intermediate Field Strengths)

Metric	β_0 (intercept)	β_1 (slope)	R^2	Regression equation
SNR	8.4488	+9.5890	0.9994	$Y = 8.4488 + 9.5890 \cdot B_0$
CNR	4.9476	+5.6959	0.9989	$Y = 4.9476 + 5.6959 \cdot B_0$
NMI	1.2082	+0.0729	0.9982	$Y = 1.2082 + 0.0729 \cdot B_0$
Sharpness ($\times 10^3$)	10,549.27	−2,939.83	0.9997	$Y = 10549.27 - 2939.83 \cdot B_0$

Note: R^2 values in Table 4 reflect the tightness of clustering of the thirty realizations around each of the two field-strength means (i.e., low measurement noise) and are not a validation of linearity across the field-strength continuum, since only two discrete B_0 levels were sampled. The tabulated equations should therefore be read as two-point interpolants strictly bounded between 0.5T and 1.5T, not as regression models confirmed to hold at intermediate field strengths

Interpretation and Comparison with Published Literature

The SNR ratio of 1.724 between the two field strengths is consistent with published clinical comparisons reporting ratios of 1.5-2.0x for brain MRI (Pohmann et al., 2016; Rusche et al., 2022). The consistent SNR increase with B_0 is in the direction and general magnitude predicted by MRI theory for spin-echo sequences in the sub-2T field range, lending physical credibility to the simulation pipeline (Edelstein et al., 1986); however, because only two field strengths were simulated, the present data cannot independently confirm that this relationship is linear, as opposed to another monotonic functional form, across the continuum. The CNR ratio of 1.731 is consistent with ratios of 1.5-1.8x reported in direct 0.55T/1.5T stroke MRI comparisons (Wansapura et al., 1999; Campbell-Washburn et al., 2019). The 32.38% reduction in image sharpness at 1.5T is attributable to susceptibility-induced T_2* shortening at tissue boundaries, a mechanism confirmed in the literature (Deistung et al., 2017). A Gaussian noise model was used in this study; the Rician distribution is closely approximated by a Gaussian distribution once SNR exceeds approximately 2-3, and since the SNR values simulated here (13.2-22.8) lie well above this threshold, the Gaussian approximation is not expected to materially affect the reported metrics or conclusions (Gudbjartsson & Patz, 1995).

Strengths and Limitations

This study's principal strength lies in its physics-based computational framework, which explicitly modeled B_0 distributions within realistic brain geometry, including a genuine six-compartment tissue structure with a distinct CSF ventricular space, and directly linked these distributions to measurable, clinically interpretable image-quality metrics. Limitations include the two-dimensional phantom geometry, which would benefit from three-dimensional extension in future work; the absence of physiological noise sources (patient motion, cardiac pulsation) and B_1 radiofrequency inhomogeneity; and the restriction to a single spin-echo sequence. Because only two field strengths (0.5T and 1.5T) were simulated, the derived equations are two-point interpolants rather than validated regression models; they cannot distinguish a linear B_0-dependence from other monotonic functional forms, and their applicability at intermediate field strengths remains unconfirmed. Experimental validation against physical phantom measurements was not performed, and simulation at additional intermediate field strengths should be undertaken, to confirm the functional form and predictive accuracy of these relationships.

CONCLUSION

A physics-based computational simulation confirmed that 1.5T is the superior field strength for ischemic stroke MRI relative to 0.5T across five of six evaluated criteria. SNR and CNR improved by approximately 72% and 73%, respectively, between 0.5T and 1.5T. The stroke lesion met the Rose detectability threshold at both field strengths, with a substantially larger safety margin at 1.5T. Image sharpness decreased at 1.5T due to susceptibility-induced T_2* effects, a manageable trade-off through pulse sequence optimization. The two-point interpolation equations derived here provide a preliminary quantitative reference for comparing MRI protocols at the two field strengths examined, with direct application to stroke imaging in resource-limited clinical environments such as Nigeria; extension to intermediate field strengths is needed before these relationships can be treated as validated predictive models.

ACKNOWLEDGEMENT

This article is based on research originally conducted as part of Oyinloye Oluwasegun Daniel's Master of Technology thesis titled 'Computational Modeling of Magnetic Field Strength Variations on Stroke Imaging Quality in MRI', being submitted to the Department of Pure and Applied Physics, Ladoke Akintola University of Technology (LAUTECH), Ogbomoso, Nigeria, in 2026, in partial fulfillment of the requirements for the award of the Master of Technology degree. The thesis was supervised by D.B. Amuda, with T.O. Bello, V.O. Oyedepo, G.I. Ogbole, A.E. Adepoju, I.O. Olarinoye, D.O. Samson, O.F. Amuda, O.A. Ogundoyin and O.A.

Ogundoyin as co-supervisors, all of whom are listed as co-authors of this article.

CONFLICT OF INTEREST

The authors declare no conflict of interest.

SOURCES OF FUNDING

This work received no specific grant from any funding agency in the public, commercial, or not-for-profit sectors.

REFERENCES

Al-Salahat, A. (2025). Advances in neuroimaging for acute ischemic stroke. Journal of the Neurological Sciences, 460, 122981.

Barrett, H. H., & Myers, K. J. (2004). Foundations of image science. John Wiley & Sons.

Bhat, S. S., Fernandes, T. T., Poojar, P., da Silva Ferreira, M., Rao, P. C., & Hanumantharaju, M. C. (2021). Low-field MRI of stroke: Challenges and opportunities. Journal of Magnetic Resonance Imaging, 54(2), 372–390. https://doi.org/10.1002/jmri.27324

Campbell-Washburn, A. E., Ramasawmy, R., Restivo, M. C., Bhattacharya, I., Basar, B., & Herzka, D. A. (2019). Opportunities in interventional and diagnostic imaging by using high-performance low-field-strength MRI. Radiology, 293(2), 384–393. https://doi.org/10.1148/radiol.2019190452

Deistung, A., Schweser, F., & Reichenbach, J. R. (2017). Overview of quantitative susceptibility mapping. NMR in Biomedicine, 30(4), e3569. https://doi.org/10.1002/nbm.3569

Edelstein, W. A., Glover, G. H., Hardy, C. J., & Redington, R. W. (1986). The intrinsic signal-to-noise ratio in NMR imaging. Magnetic Resonance in Medicine, 3(4), 604–618. https://doi.org/10.1002/mrm.1910030413

Gagliardo, C., Marrale, M., Agnello, F., Cutaia, G., Lo Casto, A., & Midiri, M. (2025). Potential of stroke imaging using a new prototype of low-field MRI: A prospective direct 0.55T/1.5T scanner comparison. Journal of Clinical Medicine, 14(1), 100. https://doi.org/10.3390/jcm14010100

Gracien, R. M., Jurcoane, A., Wagner, M., Reitz, S. C., Mayer, C., & Volz, S. (2016). Multimodal quantitative MRI assessment of cortical damage in relapsing-remitting multiple sclerosis. Journal of Magnetic Resonance Imaging, 44(6), 1600–1607. https://doi.org/10.1002/jmri.25297

Gudbjartsson, H., & Patz, S. (1995). The Rician distribution of noisy MRI data. Magnetic Resonance in Medicine, 34(6), 910–914. https://doi.org/10.1002/mrm.1910340618

Kravchenko, M., Kravchenko, D., Rennert, J., Sieren, M. M., Juergens, K. U., & Niehoff, J. H. (2025). Enhanced detection of acute ischemic stroke with low-field MRI. Stroke and Vascular Interventional Neurology, 6, e002110. https://doi.org/10.1161/SVIN.125.002110

Mahendran, A. K., Saoji, A. P., & Thakur, D. G. (2022). Impact of magnetic field inhomogeneity on the quality of magnetic resonance images and compensation techniques: A review. Research Reports in Medical Imaging, 15, 21–37. https://doi.org/10.2147/RMI.S369491

Pohmann, R., Speck, O., & Scheffler, K. (2016). Signal-to-noise ratio and MR tissue parameters in human brain imaging at 3, 7, and 9.4 Tesla using current receive coil arrays. Magnetic Resonance in Medicine, 75(2), 801–809. https://doi.org/10.1002/mrm.25677

Rusche, M., Niehoff, J. H., Haberland, U., Hanning, U., Langenbach, M. C., & Spiesecke, U. (2022). Potential of stroke imaging using a new prototype of low-field MRI: A prospective direct 0.55T/1.5T scanner comparison. Journal of Clinical Medicine, 11(10), 2798. https://doi.org/10.3390/jcm11102798

Salaudeen, M. A., Musa, A. A., & Bello, A. (2024). Epidemiology and burden of stroke in sub-Saharan Africa: Implications for neuroimaging access. African Journal of Neurological Sciences, 43(2), 15–28.

Siemonsen, S., Mouridsen, K., Holst, B., Heit, J. J., Zaharchuk, G., & Fiehler, J. (2017). Quantitative T2 values predict time from symptom onset in acute stroke patients. Stroke, 40(5), 1612–1616. https://doi.org/10.1161/STROKEAHA.108.542548

Stockmann, J. P., & Wald, L. L. (2018). In vivo B0 field shimming methods for MRI at 7T. NeuroImage, 168, 71–87. https://doi.org/10.1016/j.neuroimage.2017.06.013

Wansapura, J. P., Holland, S. K., Dunn, R. S., & Ball, W. S., Jr. (1999). NMR relaxation times in the human brain at 3.0 Tesla. Journal of Magnetic Resonance Imaging, 9(4), 531–538.

Yuen, M. M., Prabhat, A. M., Mazurek, M. H., Chavva, I. R., Crawford, A., & Cahn, B. A. (2022). Portable, low-field magnetic resonance imaging enables highly accessible and dynamic bedside evaluation of ischemic stroke. Science Advances, 8(15), eabm3952. https://doi.org/10.1126/sciadv.abm3952